Macromolecular Research, Vol. 13, No. 2, pp 107-113 (2005)

A Simulation Method for Modeling the Morphology and Characteristics of Electrospun Polymeric Nanowebs

Hyungsup Kim*, Dae-Woong Kim, and Moon Hwo Seo

Department of Textile Engineering & NITRI†, Konkuk University, 1 Hwayang, Gwangjin, Seoul 143-701, Korea

Kwang Soo Cho*

Department of Polymer Science, Kyungpook National University, 1370 Sangyeok, Buk, Daegu 702-701, Korea

Jung Rim Haw

Department of Material Science and Engineering, Konkuk University, 1 Hwayang, Gwangjin, Seoul 143-701, Korea

Received October 14, 2004; Revised December 22, 2004

Abstract: We developed an algorithm to simulate the generation of virtual nanowebs using the Monte Carlo method. To evaluate the pore size of the simulated multi-layered nanoweb, an estimation algorithm was developed using a ghost particle having zero volume and mass. The penetration time of the ghost particle through the virtual nanoweb was dependent on the pore size. By using iterative ghost particle penetrations, we obtained reliable data for the evaluation of the pore size and distribution of the virtual nanowebs. The penetration time increased with increasing number of layers and area ratio, whereas it decreased with increasing fiber diameter. Dimensional analysis showed that the penetration time can be expressed as a function of the fiber diameter, area ratio and number of layers.

Keywords: simulation, nanoweb, bead, ghost particle.

Introduction

Electrospinning is one of the most effective methods of producing nanofiber webs, and this technique uses applied high-voltage charges on polymer solutions or melts, and is considered to be the most suitable technique for industrialization among several competing nanofiber manufacturing processes. Compared with other nanofiber manufacturing processes, electrospinning has simple apparatus requirements and operating principles, and it can also be applied to many polymer solutions and melts.

Since the initial study on electrospinning was published,[1] many researches have been carried out to reveal the effects of material properties and processing parameters on the spina-bility and the resulting diameter of spun fibers using different polymers and solvents.[2-12] It was found that the fiber diameter generally decreased to a given limit as the applied voltage and the tip-to-collector distance (TCD) increased. However, the further increase of TCD results in larger fiber diameter, while higher voltages do not have any significant effect on the fiber diameter. This effect can be explained in terms of the electrical field strength on the polymer.

In addition, the effects of material parameters for various polymers and solutions has been studied in terms of concentration, viscosity, and the surface tension of the polymer solutions. The diameter of the electrospun fibers is strongly dependent on the polymer concentration and viscosity, and the surface tension of the polymer solution. Although research has provided a fundamental understanding of the process, several difficulties remain.

First, most research has focused on fiber diameter and its distribution, measured from SEM images. To obtain statistically reliable data from SEM images, it is necessary to obtain a large number of pictures from several sites in the nanoweb, and to measure the diameter of each fiber. Although this is a painstaking and time-consuming job, the data thus obtained are still unreliable, owing to the small sampling areas employed compared with the total web size.

Second, the previous studies have not provided any information on the morphology of nanowebs, which is very important for poten-tial applications, such as in filtration and wound dressings. Recently, an image analysis technique

*e-mail: iconclast@konkuk.ac.kr, polphy@knu.ac.kr

1598-5032/04/107-07

†NITRI: Next-Generation Innovative Technology Research Institute.

Table I. Variables Used in the Simulation Procedure

Variable	Description
θ_i	Contact angle between the i^{th} and $(i+1)^{th}$ bead.
d	Fiber diameter (or bead diameter composing the fiber).
n_b	Number of beads in a single fiber.
n_f	Number of fibers in a single nanoweb layer.
m	Number of layers composing the final nanoweb.
R_{area}	Area ratio, defined as the ratio of the total area of a fiber occupying the web to the total collecting area.
t_{pass}	Penetration time of a ghost particle.

has been developed for extracting valuable information using SEM images, but it is still difficult to obtain reliable data owing to the limitations of the SEM image technique, as discussed above. The focal depth of SEM micrographs also leads to another limitation of the image analysis method, because SEM micrographs usually only contain a surface image of the web. As a result, it is difficult to get precise data on the morphological parameters of a three-dimensional (3-D) web structure, such as pore size.

To provide a more precise understanding of electrospun web morphology and structure, we have developed an algorithm for simulating a nanofiber web using the Monte Carlo and estimation methods to simulate web characteristics by constructing and testing an imaginary multi-layered nanoweb. The simulation and estimation results can predict the behavior of a nanoweb using experimental research data as input.

Simulation Algorithm

Electrospun Web Generation Algorithm.

Assumptions and Variables: To simplify the simulation procedure, an ideal electrospun nanoweb was constructed using the following assumptions.

1. All the fibers composing the simulated web have the same diameter, with no variation in diameter along the fiber axis.
2. The fiber orientation distribution follows a uniform distribution, u[-π, π].
3. The final electrospun web was constructed by superposing single-layered nanowebs. As a result, the fibers do not migrate into other layers; i.e., the fiber orientation along the web thickness can be disregarded.

The variables used for the simulation procedure are summarized in Table I.

Simulation Procedure. Figure 1 shows a flowchart of the nanoweb simulation procedure using the Monte Carlo method. The procedure is composed of three iteration steps: the first iteration generates a fiber by connecting the beads, the second step forms a single-layered web by assembling

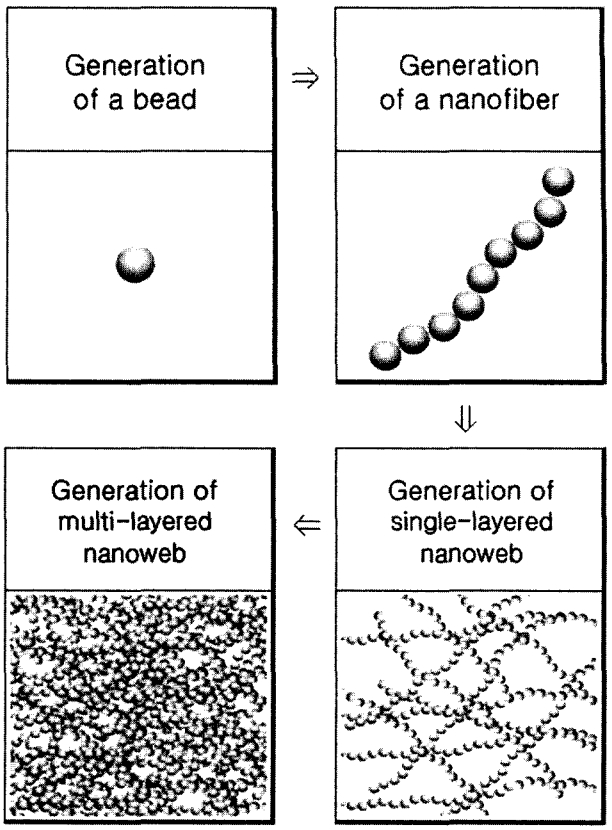

Figure 1. Nanoweb simulation procedure.

the fibers generated during the first iteration, and the third iteration assembles a multi-layered web by superposing the single-layered web produced in the second iteration.

To obtain a single nanofiber, a spherical bead having diameter d was generated at a randomly assigned location inside a two-dimensional (2-D) rectangular collecting area. The x and y coordinates of the location were assigned using a random number generator. To grow the fiber, a second bead having the same diameter as the first bead was generated at the same contacting location as the first bead, as follows.

$$x_2 = x_1 + (d \times \cos\theta_1), \quad y_2 = y_1 + (d \times \sin\theta_1) \tag{1}$$

As shown in Figure 2, the contact angle, θ_i (for $i = 1$), between the two beads was randomly selected using a computer program from a uniform distribution, $u[-\pi, \pi]$. For our purposes, it was practical to use a uniform distribution, but other types of distribution can be used in place of a uniform distribution if the orientation density function of the web is known. A third bead was generated using the same method as described above for the second bead, but using a new contact angle, θ_2. The contact angle, θ_i for $(i \geq 2)$ was selected from the range, $\theta_1 - \alpha$ to $\theta_1 + \alpha$. The angle α represents the local crimp of the fiber. Thus, the contact angle

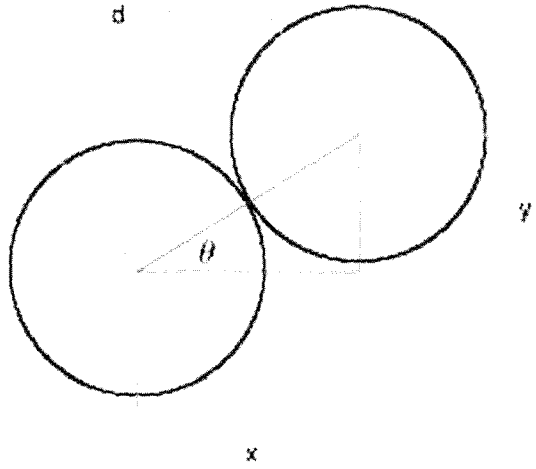

Figure 2. Fiber growth method.

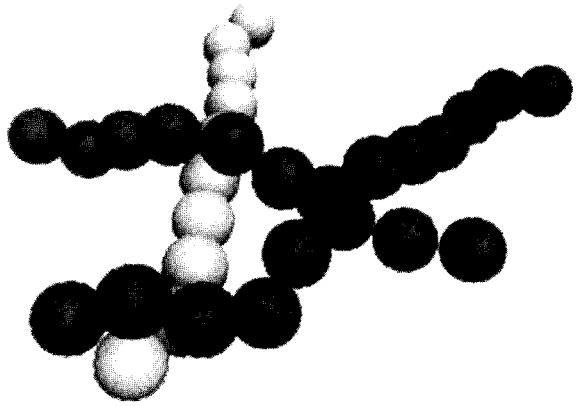

Figure 3. Overlapping of the nanofibers by volume exclusion.

represents the average orientation of the fiber, and the angle θ_l represents the local crimp of the fiber. In our simulations, we used a relatively low value of α, because the SEM images of electrospun webs from previous researches[2,4-6,8,9] showed that the fibers were almost perfectly aligned, with little observable curvature.

This fiber growth procedure was repeated for the ensuing beads for a total of n_b times. The location of the i^{th} bead was defined using eq. (2). As a result, the nanofibers composing the web were generated with a length = $n_b d$, and an average orientation angle of θ_l, as shown in Figure 3.

$$x_{i+1} = x_i + (d \times \cos\theta_i), \quad y_{i+1} = y_i + (d \times \sin\theta_i) \tag{2}$$

To create a single-layered fiber nanoweb containing n_f fibers, the single fiber generation procedure was iterated n_f times on the rectangular collecting plane. In practical electrospinning, the number of fibers in a single layer depends on the collecting speed and area, throughput, and fiber diameter. To correlate the processing and material variables, a new parameter, the area ratio (R_{area}) was introduced, defined as the ratio of the total area occupied by the fibers to the total collecting area, as shown in eq. (3):

$$R_{area} = \frac{d^2 n_b \times n_f}{A^2} \tag{3}$$

where A^2 is the total collecting area.

When the area occupied by the fibers is equal to the total collecting area, then $R_{area} = 1$. However, this does not imply that the whole collecting area is covered by fibers, because of the possibility of overlapping fibers. In general, R_{area} increases as the collecting speed decreases and the throughput increases, because the number of collected fibers increases.

Although the initial generated fiber can be deposited at any location on the collecting area without restriction, the ensuing fibers have a restriction imposed on them, because the previously generated fibers may already occupy the designated collecting area. Our simulation program directed fiber growth towards vacant spaces, wherever possible. However, the bead was classified as being out of the collecting plane if a crossover of two fibers was unavoidable, as shown in Figure 3. To avoid the sudden elevation of a bead at the crossover point, the two neighboring beads were also elevated a distance of half a bead diameter. As a result, two different beads could not have the same 3-D coordinates. The crossover of two fibers invokes a protrusion of the web, and in turn, this affects the next layer. It results in an uneven face of the simulated web, similar to that of a real electrospun web.

Because electrospun webs are usually produced using a rotating collector, the final web has a multi-layered structure. To construct a multi-layered web, we superposed the single-layered web generated using the above procedure m times to construct an m-layered nanoweb. The number of nanoweb layers directly affects the web thickness and is related to the number of collector rotations. It is noteworthy that each layer is not a simple replication of the first layer, and all layers are statistically independent.

Pore Size Estimation. Owing to the large specific surface area involved, filtration is one of the most likely applications of electrospun nanowebs. One of the most important morphological characteristics of a nanoweb for filtration is the pore size and its distribution in the web. The pore size and its distribution are correlated with the air permeation value and filtration power. We now present a method for estimating the pore size and distribution of the simulated nanowebs described above. This provides valuable information and an increased understanding of the morphological parameters and pore size of nanowebs. It can also be used to predict the pore size and its distribution of an actual electro-

spun nanoweb, if the appropriate experimental data are supplied.

We assumed an imaginary particle in the estimation procedure, denoted as a "ghost particle", having zero volume and mass. It was also assumed to be composed of a perfect elastic material. To estimate the pore size and distribution, the ghost particle was injected into the simulated nanoweb. The injected ghost particle interacted and collided with the simulated nanofibers until it exited the web. During penetration of the nanoweb, the ghost particle underwent perfectly elastic collisions with the fibers with no Brownian motion. Owing to the above assumptions, the kinetic energy of the particle was conserved, and the speed of the particle remained constant throughout the penetration. The elapsed time of particle penetration, t_{pass}, is dependent on the pore size (i.e., the diameter and length of the pore). It is self-evident that t_{pass} decreases with increasing pore size.

As described above, the fibers in the simulated nanoweb consisted of linearly connected beads. This can lead differences with a collision process involving nanofibers constructed using cylindrical fibers. To make the collision process more realistic, the fibers composed of beads needed to be enveloped into a cylindrical form, as shown in Figure 4. Instead of changing all the parts of the bead-connected fibers into cylindrical fibers, only the collision part of the fiber was transformed into the cylindrical form, as shown in Figure 4. When a particle collided with a simulated fiber, then the particle rebounded, as shown in Figure 5, and the relationship between the injecting and rebounding vectors can be expressed using eq. (4):

$$\vec{r}-\vec{x}=x_n\hat{n}+x_t\hat{t}$$

so

$$\vec{x}'-\vec{r}=-x_n\hat{n}+x_t\hat{t}=\vec{r}-\vec{x}=2x_n\hat{n} \quad (4)$$

and

$$\vec{x}'=2\vec{r}-\vec{x}=2x_n\hat{n},$$

where the unit normal vector, $\hat{n}$, can be calculated from the position of beads and the unknown coordinate x_n can also be calculated from the previous position and velocity of the ghost particle. Determination of the collision point, $\vec{r}$, can be carried out using geometric considerations of the position of the ghost particle and the related beads.

The ghost particle advances through the simulated web until it exits. We can calculate the total elapsed time (or total moving length), t_{pass}, of the ghost particle until the particle exits the simulated web. The total length is related to the pore size of the web.

By injecting the ghost particle into the same web repeatedly, we can obtain statistically reliable data on the pore size and distribution of the simulated web. The result is a useful tool for analyzing our process and the structure of a nanoweb from the relationship between the simulation data and the experimental results.

Results and Discussion

Simulation. Figure 6 shows an illustration of a single-layered nanoweb generated using the simulation program. The images of the simulated webs are similar to those of actual electrospun webs, except that the simulated fibers are composed of beads. Compared with the single-layered nanowebs, the multi-layered nanowebs are more complicated and have smaller pores.

Estimation of Pore Size. To test the estimation process and its stability, two multi-layered nanowebs with different numbers of superposed layers were constructed under the same simulation conditions. The estimation procedure was carried out over 10 replication results for each nanoweb. Each average of t_{pass} was measured and calculated by injecting 500 ghost particles into each simulated web. As shown in Figure 7, the variation of the average penetration time was relatively small in both cases, so that it is reasonable to consider our procedure to be both reliable and stable.

To reveal the effect of the geometrical parameters on the simulated nanoweb-e.g., the pore size-several webs were

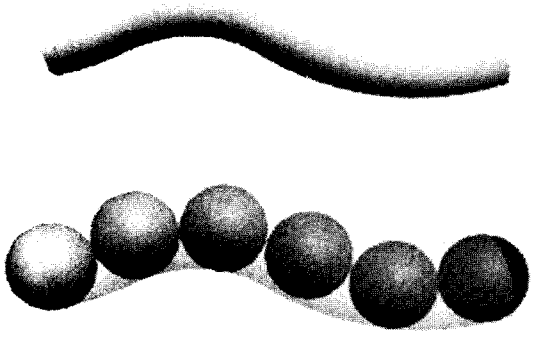

Figure 4. Enveloping of a nanofiber.

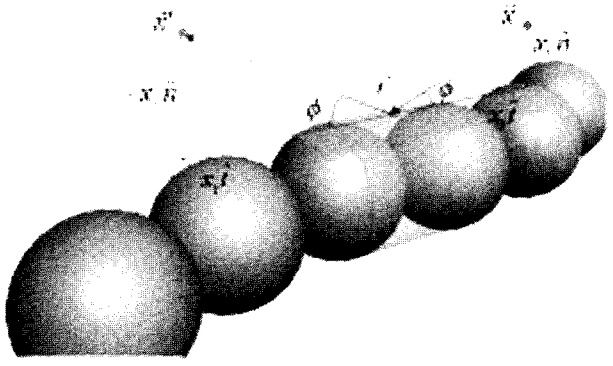

Figure 5. Collision mechanism between a fiber and a ghost particle.

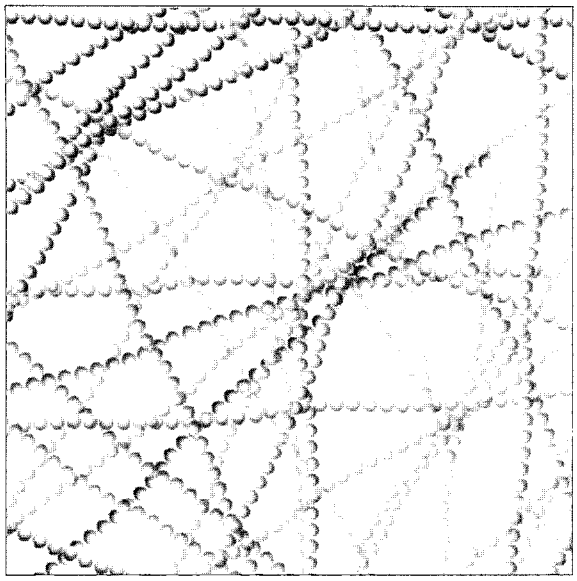

Figure 6. Single-layered nanoweb.

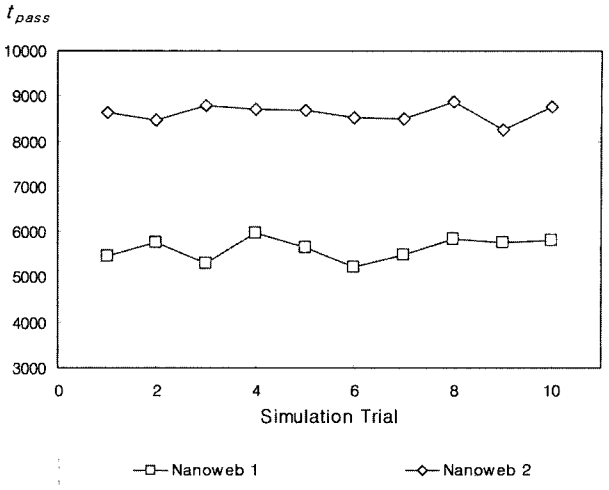

Figure 7. Average penetration time (t_{pass}) for two different number of layers. (Key: m = 10 and 20 for nanoweb 1 and 2, respectively).

generated by changing the fiber diameter and the number of layers. To estimate the pore size distribution, ghost particles were injected into different regions of the nanowebs one thousand times for each simulated web.

Figure 8 shows the penetration time distributions for three different numbers of superposed layers. The distributions are bimodal, which was a common feature of each distribution under different conditions. This observation can be explained by the web structure. When a ghost particle was injected into an open area of the web, the number of collisions was small, and the particle exited in a short time. However, a particle can be contained within the nanoweb for a longer period, and may not escape easily if injected into a dense region. Because the injected region was selected randomly using a computer program, the penetration time exhibited a bimodal distribution from statistical considerations. The heights of the peaks decreased and the distributions became more dispersed as the number of layers increased. This is not easy to explain, but it seems that the number of collisions between a ghost particle and the simulated fibers changes owing to the more complicated nanoweb structure resulting from the increased number of layers.

As shown in Figure 8, the average penetration time increases with increasing number of layers. As the number of layers increases, the nanoweb structure becomes more complex, and its thickness increases. This results in a more complicated, smaller, and longer pore structure, and this leads to an increase in penetration time.

Figure 9 shows the average penetration time change for different fiber diameters with area ratio R_{area}. The penetration time increases with increasing R_{area} for each fiber diameter. This is because the simulated nanowebs have more complex and smaller pore structures as R_{area} increases, which makes

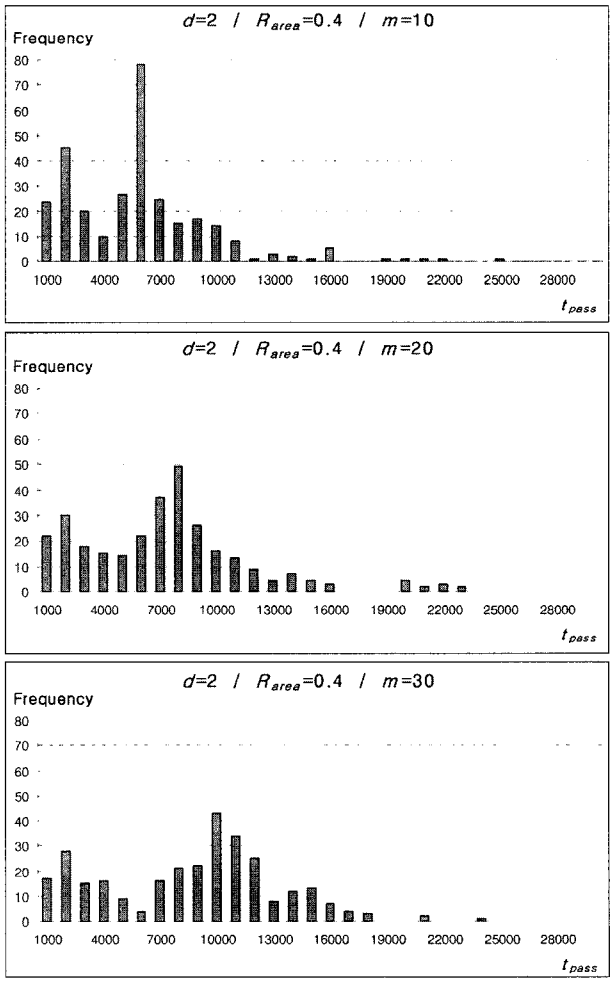

Figure 8. Penetration time distributions for different numbers of layers.

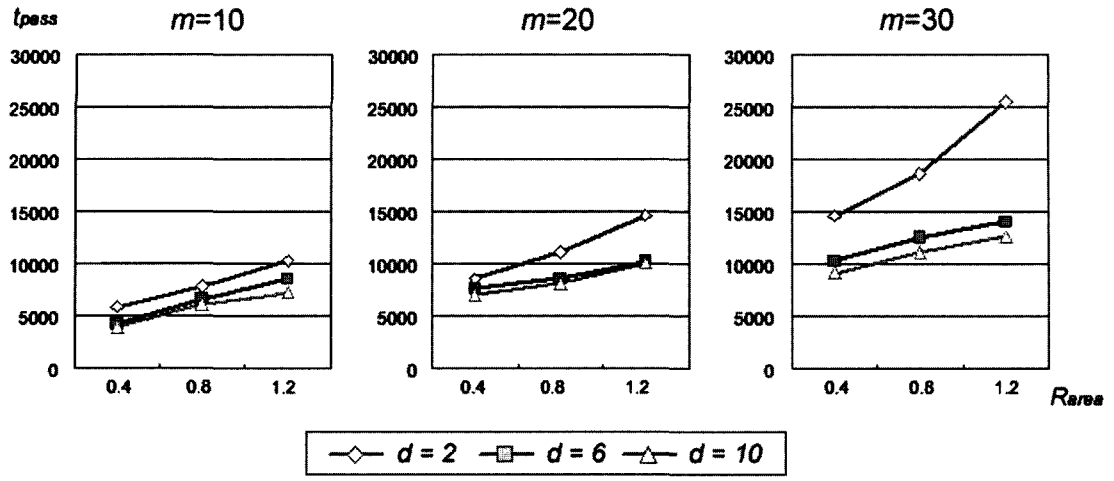

Figure 9. Effect of fiber diameter and area ratio on the penetration time.

particle penetration more difficult, and takes more time. As shown in Figure 9, the fiber diameter also significantly affected the penetration time. The particles took a shorter time to penetrate through the nanoweb with decreasing fiber diameter. The thinner fibers resulted in denser fiber packing in the nanowebs, and the volume of open areas decreased. As explained previously, the particles can then become entangled in the nanoweb, and therefore take more time to escape.

We can consider the movement of a ghost particle as being analogous to the diffusion of an ideal gas. The diffusion constant of a gas can be expressed by

$$D = \frac{L^2}{\tau} \tag{5}$$

where D is the diffusion constant, L is the characteristic length scale, and τ is the characteristic time scale. Since t_{pass} is proportional to τ and L, then the thickness of the nanoweb is proportional to the number of layers, and t_{pass} can be expressed in the form of eq. (6).

$$t_{pass} = f\left(\frac{m^2}{D}\right) \tag{6}$$

We used an unknown function in eq. (6), because the movement of a ghost particle is not exactly that of an ideal gas, and we assumed an analogous behavior. The diffusion constant of an ideal gas is given by eq. (7)[13]

$$D = \frac{1}{3}\lambda c \tag{7}$$

where λ is the mean free path of the ideal gas and c is the mean speed of the ideal gas. The mean free path, λ, scales with the fiber diameter, and it is intuitively expected that λ will be proportional to the inverse of the volume fraction of fibers in the simulation box, φ. Thus,

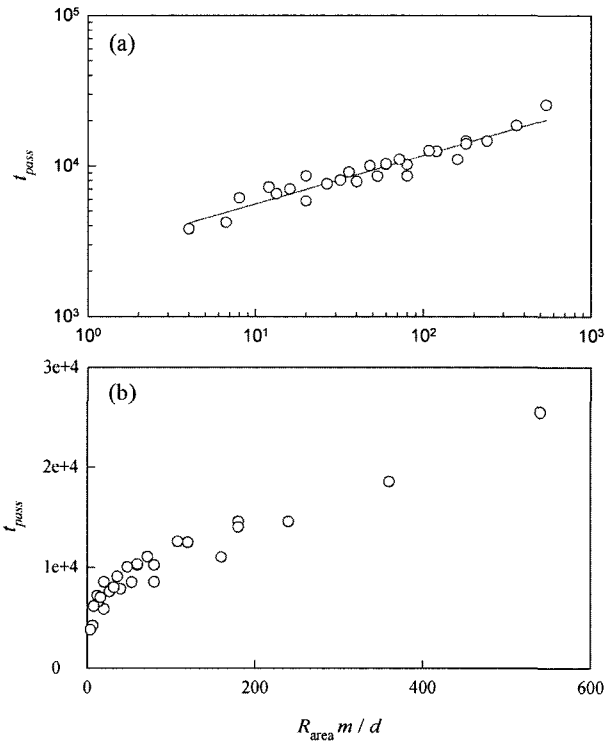

Figure 10. Penetration time plotted using data obtained from eq. (10).

$$\lambda \sim \frac{d}{\varphi} \Rightarrow D \sim \frac{d}{\varphi} \tag{8}$$

It is simple to show that the volume fraction is equal to the area ratio R_{area} in this case, since

$$\varphi = \frac{V_{fiber}}{V_{web}} = \frac{mdA^2 R_{area}}{mdA^2} = R_{area} \tag{9}$$

Thus,

$$t_{pass} = f\left(\frac{R_{area} m^2}{d}\right) \quad (10)$$

Figure 10 shows that eq. (10) is applicable, since nearly all the data points lie on a single line, irrespective of fiber diameter, area ratio, and number of layers. Figure 10 shows plots of the data shown in Figure 9. Since the mean free path is directly related to the pore size, we can say that the penetration time, t_{pass}, is strongly related to the pore size of the nanofiber web, although it is necessary to verify and correlate this with experimental data.

Conclusions

We have developed a simulation algorithm for generating nanowebs. Using the simulation program, ideal nanowebs were constructed using different morphological conditions. To evaluate the pore size of the simulated multi-layered nanowebs, an estimation algorithm was developed using a ghost particle having zero volume and mass. Using our simulation program, various nanowebs were constructed under different conditions and evaluated using the above estimation method. The penetration time was found to be strongly related to the pore size. The penetration time increased with increasing number of layer and area ratio while it decreased as the fiber diameter increased. However, quantitative relationships have to be examined using experimental data. Dimensional analysis showed that the penetration time can be expressed as a function of fiber diameter, area ratio and number of layers.

Acknowldgements. This work was supported by the Faculty Research Fund of Konkuk University, Korea in 2003.

References

(1) J. Doshi and D. H. Reneker, *J. Electrostatics*, **35**, 151 (1995).
(2) C. J. Buchko, L. C. Chen, Y. Shen, and D. C. Martin, *Polymer*, **40**, 7397 (1999).
(3) S. M. Jo, W. S. Lee, and C. W. Joo, *Fiber Technol. Indust.*, **6**, 61 (2002).
(4) J. M. Deitzel, J. Kleinmeyer, D. Harrks, and N. C. B. Tan, *Polymer*, **42**, 261 (2001).
(5) S. G. Lee, S. S. Choi, and C. H. Joo, *J. Korea Fiber Soc.*, **39**, 1 (2002).
(6) Y. S. Kang, H. Y. Kim, Y. J. Ryu, D. R. Lee, and S. J. Pack, *Polymer(Korea)*, **26**, 360 (2002).
(7) K. H. Lee, H. Y. Kim, Y. J. Ryu, K. W. Kim, and S. W. Choi, *J. Polym. Sci.; Part B: Polym. Phys.*, **41**, 1256 (2003).
(8) A. Pedicini and R. J. Farris, *Polymer*, **44**, 6857 (2003).
(9) R. Dersch, T. Liu, A. K. Schaper, A. Greiner, and J. H. Wendoff, *Fiber Soc. Fall Technical Meeting*, 54 (2002).
(10) Z. M. Huang, Y. Z. Zhang, M. Kotaki, and S. Ramakrishna, *Composite Sci. Technol.*, **63**, 2223 (2003).
(11) B. Ding, C. K. Kim, H. K. Kim, M. K. Seo, and S. J. Park, *Fiber and Polymers*, **5**, 105 (2004).
(12) K. W. Kim, K. H. Lee, M. S. Khil, Y. S. Ho, and H. K. Kim, *Fiber and Polymers*, **5**, 122 (2004).
(13) P. W. Atkins, *Physical Chemistry*, 6th ed., Oxford University Press, Oxford, UK, 1998.